This is the accepted manuscript made available via CHORUS. The article has been published as:

Freestanding silicon nanocrystals with extremely low defect content

R. N. Pereira, D. J. Rowe, R. J. Anthony, and U. Kortshagen

Phys. Rev. B **86**, 085449 — Published 27 August 2012

DOI: 10.1103/PhysRevB.86.085449

Freestanding silicon nanocrystals with extremely low defect content

R. N. Pereira*
Department of Physics and I3N, University of Aveiro, 3810-193 Aveiro, Portugal

D. J. Rowe, R. J. Anthony, and U. Kortshagen†
Department of Mechanical Engineering, University of Minnesota, Minneapolis, Minnesota 55455, USA
(Dated: July 31, 2012)

The future exploitation of the exceptional properties of freestanding silicon nanocrystals (Si-NCs) in marketable applications relies upon our ability to produce large amounts of defect-free Si-NCs by means of a low-cost method. Here, we demonstrate that Si-NCs fabricated by scalable RF plasma-assisted decomposition of silane with additional hydrogen gas injected into the afterglow region of the plasma exhibit immediately after synthesis the lowest reported defect density, corresponding to a value of only about 0.002-0.005 defects per NC for Si-NCs with 4 nm in size. In addition, the virtually perfect hydrogen termination of these Si-NCs yields an enhanced resistance against natural oxidation in comparison to Si-NCs with nearly one order of magnitude larger initial defect density.

PACS numbers: 61.46.Hk, 76.30.-v, 81.16.Pr

I. INTRODUCTION

The promise of versatile and inexpensive device fabrication associated with nanoparticle processing,[1] combined with the unique optical and electronic properties of Si at the nanoscale (such as efficient and wavelength tunable light emission[2,3] and multiple exciton generation[4]) are driving intense research on freestanding silicon nanocrystals (Si-NCs). These efforts have readily resulted in the practical demonstration of thermoelectrics,[5] solar energy to electricity conversion,[6,7] and light emission[8,9] with thin films fabricated from freestanding Si-NCs. Freestanding Si-NCs can be fabricated by various techniques, including solid-gas-reaction,[10] liquid-phase synthesis,[11,12] laser pyrolysis of silane,[13,14] laser ablation,[15] laser vaporization-controlled condensation,[16] and plasma-assisted decomposition of silane.[1,2,17,18] Several recent experimental investigations have focused on fundamental characteristics of these Si-NCs such as light emission,[2,3] electronic doping,[19,20] and optical properties.[21] Previous studies have revealed that silicon dangling bonds (Si-dbs) have an adverse impact on the Si-NC properties.[2,19,22,23] Si-dbs act as recombination and trapping centers for electrons and holes moving across Si-NC superlattices,[22,24] strongly decrease the efficiency of electronic doping with foreign impurities,[19] and have been associated with degradation of light emission from confined excitons.[2,23] Improvement of the performance of Si-NCs in (photo)electronic applications and accomplishment of new applications require the fabrication of Si-NCs with very low defect content by means of inexpensive and scalable methods. In an earlier electron spin resonance (ESR) study, we found that Si-NCs grown from the scalable method based on RF plasma-assisted decomposition of silane exhibit Si-db densities of typically 4×10^{10} cm^{-2},[25] hereafter referred to as mid initial defect density (MIDD) Si-NCs. Si-db reduction upon air exposure was observed for these MIDD Si-NCs during the so-called *induction period*, before creation of defects initiated by surface oxide shell growth.[25] After *complete* oxidation the density of defects saturates at a value of 5×10^{10} cm^{-2}.[25] Comparatively, Si-NCs grown from microwave plasma-assisted decomposition of silane[2] display typically one order of magnitude higher density of interfacial Si-dbs (5-7$\times10^{11}$ cm^{-2}) after surface oxidation in air is completed,[19,24] corresponding to 0.25-0.35 defects per NC for Si-NCs with 4 nm in size. This amount of defects may be decreased by up to one order of magnitude only after these Si-NCs are subjected to wet etching in hydrofluoric acid followed by vacuum heating at 200 °C.[24,26] Recently, highly efficient photoluminescence was observed after alkene functionalization of Si-NCs grown with injection of additional hydrogen gas into the afterglow region of a nonthermal RF plasma.[27] This enhanced photoluminescence was correlated with the presence of surface Si-H_3 species and a lower amount of defects, as suggested from a reduced ESR intensity from Si-dbs observed for these Si-NCs in comparison to Si-NCs grown with He or Ar added in the afterglow region instead of H_2.[27] The development of a production means of Si-NCs enabling defect-free NCs already immediately after synthesis, without the need of post-synthesis treatments, is of great interest in terms of reduction of device fabrication costs and processing times as well as to enhance scalability.

In the present work, we fabricate Si-NCs using silane decomposition in an RF plasma and carry out a detailed quantitative study of their defect characteristics. An extremely low defect density (7×10^{9} cm^{-2}) is found for Si-NCs grown with additional hydrogen gas injected into the afterglow region of the plasma, hereafter referred to as low initial defect density (LIDD) Si-NCs. We also compare the process of oxidation in air of the LIDD Si-NCs with that of Si-NCs containing an order of magnitude larger initial defect density (MIDD Si-NCs mentioned above), addressed in a previous study,[25] which have been grown without injection of hydrogen gas into afterglow region of the plasma. No change of defect density during

	LIDD	MIDD
Precursor gas	5% SiH_4 in He (13 sccm)	SiH_4 (6 sccm)
Carrier gas	Ar (35 sccm)	Ar (200 sccm)
Pressure	1.4 Torr	3.6 Torr
Injection gas	H_2 (100 sccm)	none
Tube I.D.	5.5 mm	22 mm
Si-NCs diameter	4.0 nm	5.5 nm

TABLE I: Synthesis conditions of the low initial defect density (LIDD) and mid initial defect density (MIDD) Si-NCs.

the *induction period* is observed for the LIDD Si-NCs. In addition, we observe improved resistance to native oxide formation for LIDD Si-NCs in comparison to MIDD Si-NCs, due to the enhanced surface hydrophobicity that results from a much reduced amount of defects on the surface and its nearly perfect hydrogen termination.

II. EXPERIMENTAL DETAILS

Freestanding spherical Si-NCs, denoted above LIDD Si-NCs, were synthesized in a flow-through reactor using a nonthermal RF (13.56 MHz) plasma. The reactor is a Pyrex tube through which silane diluted with a carrier gas is decomposed to form Si-NCs. A detailed description for the synthesis of the LIDD Si-NCs has been reported earlier,[27] so only the important features will be covered here. To prepare the LIDD Si-NCs, hydrogen gas was injected into the afterglow of the plasma and additional synthesis conditions are outlined in Table I. In this table, we also reproduce the synthesis conditions of the MIDD Si-NCs investigated earlier.[25] Experimental data presented in this work for the MIDD Si-NCs has been reported in a previous study,[25] and are reproduced here only for comparison with the LIDD Si-NCs data. The crystalline diffraction pattern of the LIDD Si-NCs was measured with a Bruker-AXS microdiffractometer with a 2.2 kW sealed Cu x-ray source. Figure 1 compares the x-ray diffraction (XRD) pattern of as-produced LIDD Si-NCs with that of the MIDD Si-NCs.[25] Using the Scherrer equation for spherical particles, NC diameters of 4.0 nm and 5.5 nm were found for the LIDD and MIDD Si-NCs, respectively. Samples were handled air-free prior to the initiation of the first measurements. Sample handling before and during measurements has been similar to that described earlier.[25] During experiments different samples were exposed to air at the same time and under the same conditions. Electron spin resonance (ESR) measurements were performed at room temperature in continuous-wave Bruker spectrometers mounted with X-band microwave bridges driven in absorption mode. In the ESR measurements, a lock-in amplifier was used with a magnetic field modulation of 100 kHz, resulting at low microwave-powers in unsaturated absorption-derivative signals with intensity proportional to the square-root of the microwave-power, as thoroughly verified by MWP series experiments. The spin-density measurements were

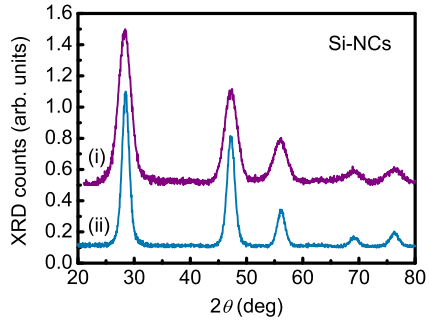

FIG. 1: XRD patterns of the (i) LIDD and (ii) MIDD Si-NCs, recorded immediately after growth.

calibrated using a diphenyl-picrylhydrazyl (DPPH) reference, magnetic field values were measured using a nuclear magnetic resonance Teslameter (resolution better than 5×10^{-3} mT), and the microwave frequency was measured with a frequency counter with resolution above 0.00001 GHz. Under these experimental conditions, spin density and g-value variations of at least 10% and 3×10^{-5}, respectively, can be distinguished. The absolute spin density accuracy is better than 30%. Fourier-transform infrared (FTIR) measurements were carried out with a nitrogen-purged Nicolet Series II Magna-IR System 750 spectrometer, equipped with a glowbar light source, a KBr beam splitter, and a mercury-cadmium-telluride detector. All absorbance spectra were recorded in diffuse reflection mode at room temperature with a resolution of 2 cm^{-1} and averaged over 100 scans. A bare gold-coated silicon wafer was used as a reference. The samples were continuously exposed to air between consecutive measurements.

III. RESULTS AND DISCUSSION

Figure 2(a) compares the ESR spectra of LIDD Si-NCs recorded within 3 minutes after air exposure with those observed for the MIDD Si-NCs.[25] The spectrum of LIDD Si-NCs [curve (i)] shows an unstructured band with zero-crossing at g=2.0054, corresponding to Si-db defects in a disordered environment.[28] For MIDD Si-NCs, a structured band was observed [curve (ii)],[25] which is well reproduced with a combination of spectra due to Si-db defects of type $P_b^{\rm NC}$ and D as described earlier.[25] ESR signal intensities were calculated by double numerical integration of the spectra recorded for different air exposure times ($t_{\rm ox}$), from which the Si-dbs densities in the Si-NCs were estimated. The results of this procedure are shown on Fig. 3. An initial defect density of 7×10^9 cm^{-2} is observed for LIDD Si-NCs, which remains approximately constant over the first 100 hours (4.2 days) of air exposure. This density corresponds to only about 0.002-0.005 defects per Si-NC, or 1 dangling bond per 200-400 Si-NCs. An increase of the defect density is observed only for $t_{\rm ox}$>100 hours, followed by a saturation at about

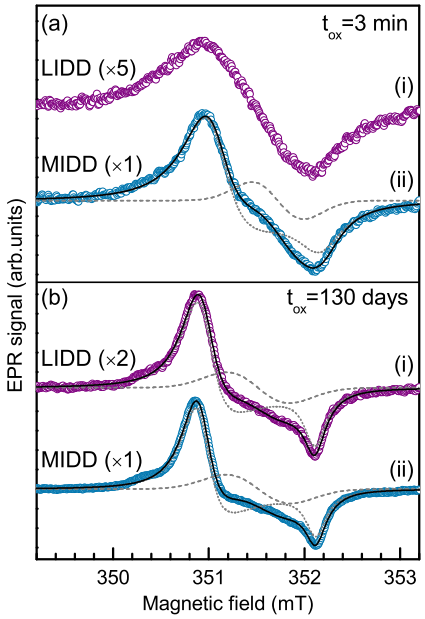

FIG. 2: ESR spectra recorded with LIDD and MIDD Si-NCs immediately after exposure of the samples to air (a) and after long term exposure to air (b). All spectra are normalized to the sample mass and multiplied by the indicated magnification factor. Solid lines correspond to computer simulations of the spectra, taking into account a powder pattern due to $P_b^{\rm NC}$ defects (dotted lines) and an isotropic resonance due to D defects (dashed lines).

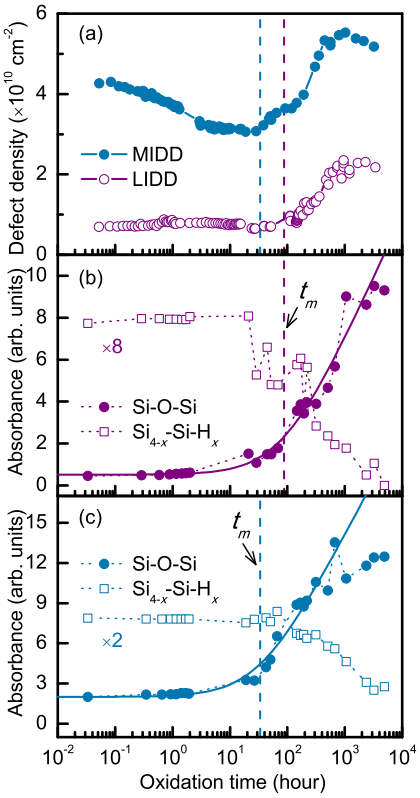

FIG. 3: (a) Dependence of the defect density measured for the LIDD and MIDD Si-NCs as a function of $t_{\rm ox}$. (b) and (c) show the variation of the intensity of FTIR bands from surface Si-O-Si and Si_{4-x}-Si-H_x species for LIDD and MIDD Si-NCs, respectively. Solid lines represent fitting curves to the Si-O-Si data using the Elovich equation.[25,29]

2×10^{10} cm^{-2} at $t_{\rm ox}\approx$800 hours (33 days). For the case of MIDD Si-NCs,[25] a defect density decrease to a minimum value of 3×10^{10} cm^{-2} was observed in the first ∼30 hours (1.25 days) of air exposure, after which an increase is observed, followed by a saturation at about 5×10^{10} cm^{-2} also at $t_{\rm ox}\approx$800 hours (33 days).[25] In Fig. 2(b), the ESR spectrum of LIDD Si-NCs recorded after *complete* oxidation is compared with that observed for MIDD Si-NCs.[25] Unlike the situation before oxidation, after *complete* oxidation the spectrum of LIDD Si-NCs is quite similar qualitatively to that observed for MIDD Si-NCs. The spectrum is also well described by a sum of the two spectral components due to $P_b^{\rm NC}$ and D centers, with g-values observed at $g_\parallel$=2.0019 and $g_\perp$=2.0086 for $P_b^{\rm NC}$ and $g_{\rm D}$=2.0053 for D centers, as previously described for the MIDD Si-NCs.[25] After *complete* oxidation the $P_b^{\rm NC}$ and D defects represent about 85% and 15%, respectively, of the total amount of defects for both the LIDD and MIDD Si-NCs. Before oxidation the $P_b^{\rm NC}$ and D defects represent about 94% and 6%, respectively, of the total amount of defects in the MIDD Si-NCs.[25] The situation is inverted for the LIDD Si-NCs, where the initial ESR band is dominated by the contribution of D defects, as revealed by its zero crossing g-value of g=2.0054, as well as its symmetric and unstructured shape. The total defect density of 7×10^9 cm^{-2} recorded before oxidation is also close to the density of D defects $[D]=4\times10^9$ cm^{-2} measured after *complete* oxidation, which indicates that the increase of the total defect density to the value of 2×10^{10} cm^{-2} is mainly due to the increase of $P_b^{\rm NC}$ defects density induced by oxidation.

In Fig. 4, the FTIR spectrum recorded for the LIDD Si-NCs within 2 minutes after air exposure is compared with that observed for the MIDD Si-NCs.[25] The spectrum of LIDD Si-NCs displays at 2000-2150 cm^{-1} a band with three components located at 2080, 2110, and 2141 cm^{-1}, attributed to Si-H stretching vibrations of Si_3-Si-H, Si_2-Si-H_2, and Si-Si-H_3 surface hydride groups, respectively.[30,31] These three components have also been distinguished in the spectrum of MIDD Si-NCs,[25] but with different relative intensities. The LIDD Si-NCs exhibit a pronounced higher order hydride concentration due to the additional hydrogen injected into the afterglow of the synthesis plasma. The MIDD Si-NCs were not treated with hydrogen injection and the hydride stretching region is similar to that observed by Winters and co-workers,[32] when their Si-NCs synthesized in a non-thermal plasma were heated to 400 °C in flight. This indicates that the Si-NC temperature for the MIDD Si-NCs remained sufficiently high immediately after synthesis in the plasma afterglow for some hydrogen desorption to occur. Similar to the situation of MIDD

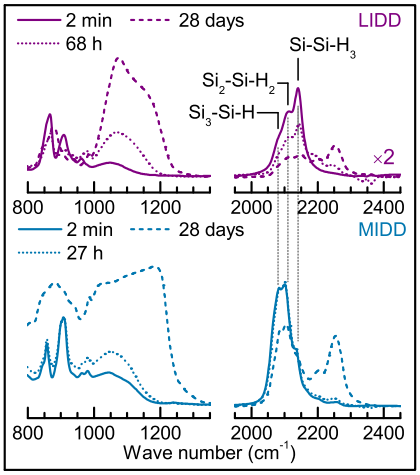

FIG. 4: FTIR spectra in the regions corresponding to stretching modes of Si-O-Si and Si-H bonds recorded for LIDD and MIDD Si-NCs immediately after exposure of the samples to air (solid lines) and after long term exposure to air (dashed lines).

Si-NCs,[25] the doublet observed for LIDD Si-NCs near 900 cm^{-1} with maxima at 866 and 908 cm^{-1} is associated with deformation modes of Si-Si-H_3 and with scissor and wag modes of Si-Si-H_2.[30,31] A relatively weak band located at ∼1030 cm^{-1} can also be revealed, due to surface Si-O-Si bonds,[1,2,22,23,33,34] most likely originating from a small contamination of the as-grown Si-NCs with oxygen, due to *in-situ* etching of the Pyrex reactor tube during synthesis, consistent with the high power necessary to achieve almost complete dissociation of the silane precursor. In the spectra recorded for the LIDD Si-NCs after a long time exposure to air (dashed lines), the intensity of the band related to Si-O-Si stretching increases strongly with a shape different from that of MIDD Si-NCs.[25] Simultaneous to changes observed in the Si-O-Si related band, the band related to Si_{4-x}-Si-H_x (x=1,2,3) hydrides decreases in intensity and a line at 2255 cm^{-1} arises, which is attributed to O_3-Si-H surface bonds.[22,33–36] The evolution of the intensity of bands from Si-O-Si and Si_{4-x}-Si-H_x, estimated by numerical integration of the spectra in the 995-1350 and 1885-2170 cm^{-1} spectral intervals, respectively, with $t_{\rm ox}$ is shown in Fig. 3(b). After an initial period of time, referred to as the *induction period*,[25,37–41] characterized by nearly no oxidation of the Si-NCs surface, the oxidation accelerates in a logarithmic fashion until it reaches saturation at $t_{\rm ox}$∼800 h, in qualitative agreement with the experimental data obtained recently for the MIDD Si-NCs,[25] and reproduced for comparison in Fig. 3(c). We have fitted the dependence of the Si-O-Si band intensity on $t_{\rm ox}$ with the Elovich equation.[25,29] The fitting curves obtained for the LIDD and MIDD samples are shown as solid lines in Fig. 3(b) and (c), respectively. From the fittings, we estimate characteristic times t_m of 88 h (3.7 days) for LIDD Si-NCs and 33 h (1.4 days) for MIDD Si-NCs. These are indicated as dashed vertical lines in Fig. 3. As can be seen in Fig. 3(a), the values t_m obtained agree very well with the time onsets of Si-db formation observed for the respective Si-NCs.

For the LIDD Si-NCs, the peak from Si-O-Si stretching shifts from 1030 cm^{-1} to 1045 cm^{-1} during the induction period, while somewhat growing in intensity. After the induction period, the Si-O-Si band starts to exhibit a higher frequency shoulder around 1145 cm^{-1}, while the main peak continues to shift to approximately 1070 cm^{-1}. Similar behavior is observed in the literature and is attributed to two mechanisms: (1) for changes in stoichiometry the main oxygen peak shifts towards higher wavenumbers, saturating at ∼1078.5 cm^{-1} for the stoichiometric SiO_2,[42] and (2) for thin films of SiO_2 a similar shift and shoulder appearance is attributed to localized compressive stress and SiO_2 restructuring.[43] For the MIDD sample, a growth and shift of the main peak similar to those observed for the LIDD Si-NCs is observed during the induction period. However, after the induction period the higher frequency shoulder gradually overtakes the peak initially at 1026 cm^{-1}.

Our combined ESR and FTIR data enable us to draw the following important conclusions. In the case of LIDD Si-NCs, the majority of surface Si-dbs present at the newly formed Si-NC surface are passivated by hydrogen gas injected into the plasma afterglow, resulting in a very low initial defect density (0.002-0.005 defects per NC). Remarkably, this value is about 30 times lower than that observed for H-terminated Si-NCs grown from microwave plasma assisted decomposition of silane.[24,26] The dangling bonds which are present in the as-produced Si-NCs are in fact most likely located on sites inaccessible to hydrogen, i.e. are not located close to the Si-NCs surface. This is also consistent with fact that the ESR signal reveals mostly D defects, as shown Fig. 2(a), which are typically Si-dbs located on internal sites. Such in-flight passivation of surface Si-dbs does not take place in MIDD Si-NCs, resulting in the considerably larger density of defects observed (4×10^{10} cm^{-2}) and a markedly different shape of the ESR spectra, due to the presence of surface defects of type $P_b^{\rm NC}$ in addition to the residual internal D defects [Fig. 2(a)]. For MIDD Si-NCs, the decrease of the intensity of the ESR spectrum during the induction period shows that the amount of $P_b^{\rm NC}$ (superficial) defects decreases.[25] This decrease has been associated with (i) an effective passivation of the defects, via e.g. the reaction $Si_3{\equiv}Si{\bullet}+H_2O{\rightarrow}Si_3{\equiv}Si\text{-}OH+H$, or (ii) a charge transfer process that changes the valence state of the $P_b^{\rm NC}$ defects to a charged (diamagnetic) state.[25] The absence of a defect density decrease for the LIDD Si-NCs may be understood based on the mechanism (i). For LIDD Si-NCs, the amount of superficial $P_b^{\rm NC}$ defects is negligible and the residual Si-dbs present (D defects) are not accessible to H_2O. Therefore, the reaction $Si_3{\equiv}Si{\bullet}+H_2O{\rightarrow}Si_3{\equiv}Si\text{-}OH+H$ does not take place, resulting in a quite stable density of Si-dbs throughout the entire induction period.

In Fig. 3, we show that the values t_m obtained from

fitting the FTIR data agree very well with the onset of increasing Si-db formation observed for the respective Si-NCs, providing further support to the conclusion that the creation of interfacial Si-db defects is directly linked to the formation of surface Si-O-Si bonds.[25] It is interesting to note that the LIDD Si-NCs display a much longer induction period of t_m=88 h (3.7 days) when compared to MIDD Si-NCs (1.4 days). This difference should not result from the differences in size of the NCs in the two samples. In previous studies, shorter induction periods have been observed for nanoparticles (curved Si surface) in comparison to flat surfaces of bulk silicon,[44] due to the increasingly higher number of oxidation sites present in increasingly curved surfaces. Thus, the somewhat smaller size of the NCs in the LIDD samples would result in a shortened induction period in comparison to MIDD Si-NCs, which is in clear contrast with our experimental results. Therefore, the longer induction period observed for the LIDD Si-NCs should have another origin. For ambient-air oxidation of bulk-Si surfaces, values ranging from 3 to 170 h have been found, depending on the Si surface index, air humidity, and the initial amount of residual Si-OH groups at the surface.[37–41] According to the Cabrera-Mott mechanism of ambient-air oxidation of bulk-Si and Si-NC surfaces,[20,33,45] the oxidation is initiated by adsorption of water molecules at surface Si-OH groups followed by cleavage of Si-Si backbonds of Si-OH. This is followed by electron transfer from the broken bond to an adsorbed O_2 molecule, which drifts toward the cleaved bond, leading to the oxidation of this bond and of a neighboring Si-Si bond.[45] The sequence of steps involved in the ambient-air oxidation of Si-NCs can be seen in reference [25]. The steps prior to the formation of Si-O-Si take place during the induction period and a larger amount of surface Si-OH groups results in a shorter t_m.[40,41] Thus, the large difference in t_m observed for LIDD and MIDD Si-NCs should originate from a smaller surface contamination of the LIDD Si-NCs with Si-OH groups. This is also supported by our FTIR data, where we observe the presence of surface Si-OH bonds only for the MIDD Si-NCs. The differences observed in the initial behavior of the defect density immediately after air exposure between LIDD and MIDD Si-NCs may also elucidate this issue. As mentioned above, in the case of MIDD Si-NCs an initial decrease of the defect density is observed, which could be due to the reaction $Si_3{\equiv}Si{\bullet}+H_2O{\rightarrow}Si_3{\equiv}Si\text{-}OH+H$, resulting in a contamination of the NCs surface with Si-OH groups. This defect density reduction upon air exposure is not observed for LIDD, which could indicate a smaller surface contamination in this case.

Lastly, we can use the ESR data to elucidate the differences in the time evolution of the Si-O-Si band as measured in FTIR. In the LIDD sample, the low frequency peak shifts to higher energy and increases in intensity, consistent with increasing stoichiometry of the surface silicon oxide. This is likely the case, as it is reasonable to believe that a complete oxide monolayer does not form until the end of the induction period and the onset of defect creation. Then, as the oxide layer grows, additional oxygen incorporation causes compressive stress to form in the surface layer, which is consistent with the appearance of the high frequency shoulder in the Si-O-Si band. For the MIDD Si-NCs, since more defects are present initially, more sites are available for oxygen incorporation and a larger amount of disorder is present in the oxide layer. This causes a much larger compressive stress to form, even though the defect creation rate remains the same as that of the LIDD sample, consistent with the much larger and dominant high frequency shoulder in the Si-O-Si band of the MIDD sample.

IV. CONCLUSIONS

Using ESR, we compared the defect characteristics of freestanding Si-NCs fabricated under two different conditions based on silane decomposition in an RF plasma and their evolution upon exposure to ambient air conditions. We found that Si-NCs grown with additional hydrogen gas injected into the afterglow region of the plasma exhibit an extremely low defect density of only about 0.002-0.005 defects per Si-NC, measured immediately after synthesis, which corresponds to about a six-fold improvement with respect to the best values reported so far. Quite distinct behavior upon air oxidation was observed between these LIDD Si-NCs and Si-NCs grown under different conditions and with nearly one order of magnitude larger initial defect density (MIDD Si-NCs). LIDD Si-NCs display improved resistance against surface oxide formation due a reduction of the catalytic effect of water molecules on the natural oxidation, which results from a virtually perfect hydrogen termination of the NCs surface, predominantly in the form of $Si\text{-}H_3$ species, and reduced amount of surface defects.

ACKNOWLEDGMENTS

DJR and RJA were primarily supported by the MRSEC program of the National Science Foundation (NSF) under Award Number DMR-0819885. This program is also acknowledged for supporting a working visit of RNP to the University of Minnesota. Part of this work was carried out in the College of Science and Engineering Characterization Facility, University of Minnesota, which has received capital equipment funding from the NSF through the MRSEC, ERC, and MRI programs, in the College of Science and Engineering and Nanofabrication Center, University of Minnesota, which receives partial support from NSF through the NNIN program, and at the Institute for Nanostructures, Nanomodelling and Nanofabrication in Portugal with funding from the HybridSolar Project and PEst-C/CTM/LA0025/2011. The authors would also like to acknowledge the Biophysical Spectroscopy Facility, University of Minnesota, Dr.

David D. Thomas and Ryan Mello for their support with ESR apparatus, and Ryan Gresback for his support with experiments.

* Electronic address: rnpereira@ua.pt
† Electronic address: uk@me.umn.edu

[1] L. Mangolini and U. Kortshagen, Adv. Mater. **19**, 2513 (2007).
[2] A. Gupta, M. T. Swihart, and H. Wiggers, Adv. Funct. Mater. **19**, 696 (2009).
[3] D. Jurbergs, E. Rogojina, L. Mangolini, and U. Kortshagen, Appl. Phys. Lett. **88**, 233116 (2006).
[4] M. C. Beard, K. P. Knutsen, P. Yu, J. M. Luther, Q. Song, W. K. Metzger, R. J. Ellingson, and A. J. Nozik, Nano Lett. **7**, 2506 (2007).
[5] R. Lechner, H. Wiggers, A. Ebbers, J. Steiger, M. S. Brandt, and M. Stutzmann, Phys. Status Solidi RRL **1**, 262 (2007).
[6] C.-Y. Liu, Z. C. Holman, and U. R. Kortshagen, Nano Lett. **9**, 449 (2009).
[7] C.-Y. Liu, Z. C. Holman, and U. R. Kortshagen, Adv. Funct. Mater. **20**, 2157 (2010).
[8] K.-Y. Cheng, R. Anthony, U. R. Kortshagen, and R. J. Holmes, Nano Lett. **10**, 1154 (2010).
[9] K.-Y. Cheng, R. Anthony, U. R. Kortshagen, and R. J. Holmes, Nano Lett. **11**, 1952 (2011).
[10] J. Acker, K. Bohmhammel, E. Henneberg, G. Irmer, I. Röver, and G. Roewer, Adv. Mater. **12**, 1605 (2000).
[11] J. R. Heath, Science **258**, 1131 (1992).
[12] R. A. Bley and S. M. Kauzlarich, J. Am. Chem. Soc. **118**, 12461 (1996).
[13] G. Ledoux, O. Guillois, D. Porterat, C. Reynaud, F. Huisken, B. Kohn, and V. Paillard, Phys. Rev. B **62**, 15942 (2000).
[14] X. Li, Y. He, S. S. Talukdar, and M. T. Swihart, Langmuir **19**, 8490 (2003).
[15] V. Švrček, T. Sasaki, Y. Shimizu, and N. Koshizaki, Appl. Phys. Lett. **89**, 213113 (2006).
[16] S. Li, S. J. Silers, and M. S. El-Shall, J. Phys. Chem. B **101**, 1794 (1997).
[17] L. Mangolini, E. Thimsen, and U. Kortshagen, Nano Lett. **5**, 655 (2005).
[18] Y. Kanemitsu, S. Okamoto, M. Otobe, and S. Oda, Phys. Rev. B **55**, R7375 (1997).
[19] A. R. Stegner, R. N. Pereira, R. Lechner, K. Klein, H. Wiggers, M. Stutzmann, and M. S. Brandt, Phys. Rev. B **80**, 165326 (2009).
[20] X. D. Pi, R. Gresback, R. W. Liptak, S. A. Campbell, and U. Kortshagen, Appl. Phys. Lett. **92**, 123102 (2008).
[21] V. G. Kravets, C. Meier, D. Konjhodzic, A. Lorke, and H. Wiggers, J. Appl. Phys. **97**, 084306 (2005).
[22] A. R. Stegner, R. N. Pereira, K. Klein, R. Lechner, R. Dietmueller, M. S. Brandt, M. Stutzmann, and H. Wiggers, Phys. Rev. Lett. **100**, 026803 (2008).
[23] X. D. Pi, L. Mangolini, S. A. Campbell, and U. Kortshagen, Phys. Rev. B **75**, 085423 (2007).
[24] S. Niesar, A. R. Stegner, R. N. Pereira, M. Hoeb, H. Wiggers, M. S. Brandt, and M. Stutzmann, Appl. Phys. Lett. **96**, 193112 (2010).
[25] R. N. Pereira, D. J. Rowe, R. J. Anthony, and U. Kortshagen, Phys. Rev. B **83**, 155327 (2011).
[26] S. Niesar, A. R. Stegner, R. N. Pereira, M. Hoeb, H. Wiggers, M. S. Brandt, and M. Stutzmann, Adv. Funct. Mater. **22**, 1190 (2012).
[27] R. J. Anthony, D. J. Rowe, M. Stein, J. Yang, and U. Kortshagen, Adv. Funct. Mater. **21**, 4042 (2011).
[28] M. Stutzmann and D. K. Biegelsen, Phys. Rev. B **40**, 9834 (1989).
[29] C. Aharoni and F. C. Tompkins, Adv. Catal. **21**, 1 (1970).
[30] J. Holm and J. T. Roberts, J. Am. Chem. Soc. **129**, 2496 (2007).
[31] D. C. Marra, E. A. Edelberg, R. L. Naone, and E. S. Aydil, J. Vac. Sci. Technol. A **16**, 3199 (1998).
[32] B. J. Winters, J. Holm, and J. T. Roberts, J. Nanopart. Res. **13**, 5473 (2011).
[33] R. W. Liptak, U. Kortshagen, and S. A. Campbell, J. Appl. Phys. **106**, 064313 (2009).
[34] W. Theiss, Surf. Sci. Rep. **29**, 91 (1997).
[35] Y. Kato, T. Ito, and A. Hiraki, Jpn. J. Appl. Phys. **27**, L1406 (1988).
[36] G. Lucovsky, J. Yang, S. S. Chao, J. E. Tyler, and W. Czubatyj, Phys. Rev. B **28**, 3225 (1983).
[37] M. R. Houston and R. Maboudian, J. Appl. Phys. **78**, 3801 (1995).
[38] D. Gräf, M. Grundner, R. Schulz, and L. Mühlhoff, J. Appl. Phys. **68**, 5155 (1990).
[39] D. Bodlaki and E. Borguet, J. Appl. Phys. **95**, 4675 (2004).
[40] T. Miura, M. Niwano, D. Shoji, and N. Miyamoto, J. Appl. Phys. **79**, 4373 (1996).
[41] M. Niwano, J. Kageyama, K. Kurita, K. Kinashi, I. Takahashi, and N. Miyamoto, J. Appl. Phys. **76**, 2157 (1994).
[42] J. T. Fitch, S. S. Kim, and G. Lucovsky, J. Vac. Sci. Technol. A **8**, 1871 (1990).
[43] E. San Andrés, A. del Prado, F. L. Martínez, I. Mártil, D. Bravo, and F. J. López, J. Appl. Phys. **87**, 1187 (2000).
[44] D.-Q. Yang, J.-N. Gillet, M. Meunier, and E. Sacher, J. Appl. Phys. **97**, 024303 (2005).
[45] G. F. Cerofolini, D. Mascolo, and M. O. Vlad, J. Appl. Phys. **100**, 054308 (2006), and references therein.